Aqueous Solutions of Ionic Liquids: Study of the Solution/Vapor Interface using Molecular Dynamics Simulations

Jan Picálek,[1] Babak Minofar,[2] Jiří Kolafa,[1] and Pavel Jungwirth[2*]*

[1]Department of Physical Chemistry, Institute of Chemical Technology, Prague; Technická 5, 16628 Praha 6, Czech Republic.

[2]Institute of Organic Chemistry and Biochemistry, Academy of Sciences of the Czech Republic, and Center for Complex Molecular Systems and Biomolecules; Flemingovo nám. 2, 16610 Prague 6, Czech Republic.

[*]Corresponding authors: jiri.kolafa@vscht.cz (J. K.) and pavel.jungwirth@uochb.cas.cz (P. J.)

We performed a detailed molecular dynamics study of the interfacial structure of aqueous solutions of 1-butyl-3-methylimidazolium tetrafluoroborate and 1-butyl-3-methylimidazolium hexafluorophosphate in order to explain the anomalous dependence of the surface tension on concentration. Both nonpolarizable and polarizable force fields have been employed. The initial decrease of surface tension was confirmed for both systems, while the increase at higher bulk concentrations was observed only for the more hydrophilic tetrafluoroborate anion. Propensity of butyl chains toward vacuum, the preferably parallel orientation of imidazolium rings, and the local balance of cations and anions at the surface layer were observed in accordance with experiment. Most surface phenomena are more pronounced if polarizability is taken into account.

Keywords: polarizability, force field, 1-butyl-3-methylimidazolium, tetrafluoroborate, hexafluorophosphate

1. Introduction

Ionic liquids (IL) or more precisely room-temperature ionic liquids (RTIL) are defined as salts that are molten at ambient conditions. They have attracted interest in recent years due to their favorable chemical and physical properties[1], being thermally stable solvents with negligible vapor tension at room temperature. ILs have been shown to have applicability in a wide range of areas including separation processes, catalysis and electrochemistry.[2] A typical IL consists of an organic cation and an inorganic anion. The most extensively studied family of ILs contains 1-alkyl-3-methylimidazolium cation combined with PF_6^-, BF_4^-, Cl^-, etc.

A number of experiments have been carried out to gain fundamental understanding of bulk properties of ionic liquids.[1] Although less frequent, several studies focused also on characterization of surfaces of ionic liquids including direct recoil spectroscopy[3], neutron and X-ray reflection[4,5,6], surface tension[5,7,8] and sum-frequency spectroscopy.[7,9,10] Corresponding theoretical studies include quantum chemistry calculations[11,12], MD simulations of the IL/water/gas interface[13–16] and MD simulations of IL/gas interface[17,18,19]. For the purposes of MD simulations a number of force fields have been developed either on the basis of the Lennard-Jones potential[20–29] or the Buckingham (exp-6) potential.[20]

In this study we focus on surfaces of aqueous solutions of ILs. Interfacial properties of simple salts dissolved in water have been documented to be different than those in bulk with strongly specific surface ion propensities.[31,32,33] The situation is expected to be even more intricate for ILs dissolved in water, since ILs involve more bulky complex ions. Here, different effects such as hydrophobicity, polarization, interactions with counter-ions, etc., can contribute to the surface behavior of these ions.

Properties of the IL-water interfaces may be strongly influenced by the nature of the cation and the anion. Ionic liquids containing anions such as PF_6^-, AsF_6^- or Tf_2N^- are hydrophobic, while those with anions like BF_4^-, NO_3^- or ClO_4^- are water miscible.[1] Water molecules preferentially interact with anions[34] and the interface is strongly structured. In the case of pure imidazolium-based ionic liquids, the aromatic rings of the cations are preferentially aligned along to the surface and the butyl chains point into vacuum.[10,35] The effect of temperature and the choice of the anion on the cationic orientation is small.[18,36] Water affects the surface of hydrophobic ionic liquids more than the surface of the hydrophilic ones. The cationic ring of the hydrophobic ionic liquids is reoriented along to the surface normal but remains parallel for the hydrophilic ones.

Bowers and co-workers[5] investigated the influence of water contents on the surface tension of aqueous solutions of imidazolium-based ionic liquids. An unusual increase of surface tension attributed to aggregation behavior was found. Sung and co-workers[7] related this phenomenon to bulk-surface exchange of the anion. They suggested that the anion is being desolvated from the bulk and occupies the surface.

Here, we aim at understanding of this phenomenon at a molecular level. To this end we performed a detailed molecular dynamics study of the interfacial structure of aqueous solutions of 1-butyl-3-methylimidazolium tetrafluoroborate ($BMIMBF_4$) and 1-butyl-3-methylimidazolium hexafluorophosphate ($BMIMPF_6$). MD simulations have potential pitfalls, many of them caused by inaccuracies of the employed interaction potential. An important question in this context is whether the usual pairwise-additive force fields ignoring polarizability are suitable to model fluids dominated by electrostatic interactions like ionic liquids. Inclusion of polarizability was found to be important in the case of pure 1-ethyl-3-methylimidazolium nitrate[19,30], as well as for an accurate description of simple inorganic salts/water interfaces.[32] In the present study we compare results for aqueous ILs obtained

using a non-polarizable vs. polarizable force fields and discuss the effect of polarizability on the interfacial properties.

2. Computational Details

MD simulations were performed using both non-polarizable and polarizable force fields.

2.1. MD with a non-polarizable force field

Ionic liquids $[BMIM]^+[BF_4]^-$ and $[BMIM]^+[PF_6]^-$ were modeled by an all-atom pairwise force field.[28] For water we used the new TIP4P/2005 model tailored to condensed phase calculations.[37]

The standard slab geometry [38] was used for the interface. The slab is perpendicular to the *z*-axis of the simulation cell which is periodic in the *x* and *y* directions. The sizes of the simulation box were fixed during simulation (NVT ensemble). The height (*z*-dimension) to width (*x* and *y*-dimensions) ratio was 2. In order to minimize the influence of finite-size effects (capillary waves)[39] on the comparison of results at different concentrations, we tried to keep the box dimensions the same. At low concentrations (a few molecules of IL) this could be satisfied only approximately; the *x*- and *y*-sizes of the box were in the range of 36–45 Å. Long-range Coulombic interactions were accounted for by the 3D Ewald summation method[40] with the slab dipole corrected for[41], although test calculations have shown that the impact of this correction to final results is marginal. The Lennard-Jones cutoff (see Eq. (9)) was set to 12 Å, and the corrections to the surface tension were calculated using *z*-density profiles, see the Appendix. Temperature was kept at 360 K by the Berendsen (friction) thermostat with the correlation time set to 2 ps. The equations of motion were integrated using the Verlet method

with a timestep of 2 fs and bond lengths constrained by SHAKE. Note that these thermostat and integrator settings lead to a small equipartition error; a typical kinetic temperature calculated from translational degrees of freedom is by about 1 K higher then the thermostat temperature while the "internal" (rotational and vibrational) temperature is by about the same amount lower. Molecular dynamics simulations were performed by the molecular modeling and simulation package MACSIMUS.[42]

The box dimensions were chosen so that the overall density of the inhomogeneous system was 0.5 g cm^{-3}, which means that about half of the box is occupied by the slab. The initial configuration was a lattice with a low density. The box size was gradually rescaled until the slab system reached the desired estimated bulk density. To create a slab, additional forces were applied. The system was intensely cooled during the initialization (the thermostat correlation time was set to 0.1 ps). After developing a stable slab, these forces were turned off and only forces preventing particles to move periodically in the *z*-direction (which occurs rarely for volatile water) were applied. Then the system was equilibrated for 600 ps, after which production runs lasting 3 ns or longer were started; in some cases, several independent runs were performed and the results averaged. The thermodynamic properties of the system (total energy, pressure, temperature, kinetic and potential energy contributions, etc.) were saved every 0.01 ps for further analysis.

2.2. Surface tension

The surface tension is defined as

$$\gamma = \left(\frac{\partial A}{\partial S}\right)_{T,V} \qquad (1)$$

where S is the surface area and

$$A = -kT \ln \left[\int \exp[-\beta U] \, \mathrm{d}\vec{r}^N \right] \tag{2}$$

is the residual Helmholtz free energy. The partial derivative in Eq. (1) must be calculated at constant volume which is best accomplished by using rescaled coordinates (marked by underlined symbols) keeping the volume V as well as the volume element $\mathrm{d}r_i = \mathrm{d}\underline{r}_i$ constant,

$$\vec{r}_i = ((S/2)^{1/2}\underline{x}_i, (S/2)^{1/2}\underline{y}_i, (S/2)^{-1}\underline{z}_i) \tag{3}$$

Note that there are two surfaces in the slab and therefore $S/2=L_xL_y$, where L_x, L_y, L_z are the dimensions of the periodic simulation box. The resulting surface tension is

$$\gamma = \left(\frac{\partial A}{\partial S}\right)_{T,V} = \left(\frac{\partial A}{\partial S}\right)_{T,\underline{\vec{r}}^N} = \frac{1}{2S}\left\langle \sum_i (x_i, y_i, -2z_i) \cdot \left(\frac{\partial U}{\partial \vec{r}_i}\right) \right\rangle \tag{4}$$

In case of pair forces, $U = \sum_{i<j} u_{ij}(r_{ij})$, this equation adopts the well-known form**[**39**]**

$$\gamma = \frac{1}{4L_xL_y}\left\langle \sum_{i<j} u'_{ij}(r_{ij}) \, \frac{x_{ij}^2 + y_{ij}^2 - 2z_{ij}^2}{r_{ij}} \right\rangle \tag{5}$$

or in terms of the pressure tensor[43]

$$\gamma = \frac{1}{2} L_x \left\langle P_{zz} - \frac{P_{xx} + P_{yy}}{2} \right\rangle \tag{6}$$

In the Ewald summation method, the formulas are more complicated. However, if the vapor pressure is negligible, one can neglect the z-component of the pressure tensor and replace $-2z_i$ in (4) by $+z_i$; a small vapor pressure P^s can be easily corrected for if necessary. Finally, we get

$$\gamma = -\frac{3L_z}{4}(P - P^{\mathrm{s}}) \tag{7}$$

where P is the "pressure" formally calculated by the same formula as in the homogeneous

system, particularly with the virial of electrostatic forces replaced by the electrostatic energy as follows from the virial theorem.

2.3. MD with a polarizable force field

Polarizable molecular dynamics simulations of aqueous solutions of the ionic liquid $[BMIM]^+[BF_4]^-$ were also performed in the slab geometry.[38] We used a unit cell which contained 863 water molecules. The global mole fraction of the ionic liquid solute varied from 0.002 to 0.05. The size of the square box unit cell was approximately 30×30×100 Å, and the 3D periodic boundary conditions were applied.[40]

Non-bonded interactions were cut off at 12 Å with long-range electrostatic interactions accounted for using the particle mesh Ewald procedure.[44] A time step of 1 fs was employed and all bonds involving hydrogen atoms were constrained using the SHAKE algorithm.[45] Systems were first subjected to energy minimization for removing possible bad contacts and then equilibrated for 500 ps. Production runs of at least 1.5 ns were performed in the NVT ensemble at 300 K.

For these simulations a polarizable force field was employed. For $[BMIM]^+$ and $[BF_4]^-$ we used the general amber force field parameter set[46] while for water the POL3 model was employed.[47] Partial charges for the ions were evaluated with the standard RESP procedure.[48] Polarizable molecular dynamics simulations were performed using the Amber 8 program and the induced dipoles were converged in each step using a self-consistent procedure with the default convergence criterion.[49]

4. Results and Discussion

4.1. MD with a non-polarizable force field

The density profiles (i.e., histogrammed distributions of selected atoms of the IL across the slab) collected in Figs. 1 and 2 give us the first insight into the structure of the interface. It can be seen that the ions are preferentially concentrated at the surface, especially at the low concentration (i.e., they act as surfactants). The density profiles are somewhat asymmetric, which is an artifact of the process of equilibration; namely, ions initially distributed randomly in the bulk move toward the surface, but to dissolve again in the bulk and diffuse to the opposite side of the slab takes too long. However, this effect is not dramatic, particularly at higher IL concentrations where sampling is improved. The peaks of cations and anions are approximately at the same position reflecting the overall charge neutrality. The peaks of ending carbons of the butyl chain are shifted by about 4 Å toward vacuum. Mainly butyl chains thus cover the surface. At high concentrations, a layer laying 5–10 Å below this enriched layer is depleted of butyls. Almost all chains thus point toward vacuum.

More details of the charge distribution are apparent from charge density profiles, both of individual atoms and the total charge density profile (see Figs. 3 and 4). At higher concentrations the cations and anions effectively compensate each other. The total charge density profile (averaged charge profile across the slab) shows a small surplus of positive charge at the surface (of surface charge density roughly 0.001 e/Å^2) followed by a negatively charged subsurface layer (surface density of dipole moment is about 0.03 D/Å^2); this is the same behavior as observed for pure water. At lower concentrations there are slightly more cations at the surface than anions and this difference is partly compensated by orientation of water dipoles, in accordance with the observations of Sung et al.[7] (the BF_4^- anions start to

appear at the surface from mole fraction 0.016 until the anions and cations are equally populated at 0.05 or higher). The total charge density profile is nevertheless similar to that for higher concentrations. In other words, the solvation of ions is slightly asymmetric near the surface.

The orientation of the cations at the surface can be quantified by averaged values of the Legendre polynomials. The cosine (i.e., the first Legendre polynomial) of the angle α between the elongated cation (the vector from the ring center to the terminal methyl of the butyl), and the normal to the surface shows again the preferential orientation of the butyl chains toward vacuum. To determine the orientation of the imidazolium-ring, the second Legendre polynomial (of the cosine of the ring–surface angle β) is needed, see Figs. 5 and 6. At the surface layer this second Legendre polynomial is positive which means that the ring is preferentially parallel to the surface, in agreement with experiment.[10,35]

Hydrogen bonding patterns at the interface and the energy/entropy interplay connected with the hydrogen-bond network can be analyzed by the concept of dangling hydrogens. A dangling hydrogen is defined as a hydrogen which is not engaged in any hydrogen bond; a hydrogen bond is defined for this purpose (from several available definitions) as an intermolecular O–H pair closer than 2.45 Å (this is a position of a deep minimum on the O–H correlation function). For pure water the number of dangling hydrogens at the surface layer is approximately twice the bulk value. The presence of ionic liquids slightly increases the concentration of dangling hydrogens in the bulk fluid but decreases it at the surface layer (another reason for the ionic liquid to move to the surface) so that the distribution is almost uniform across the slab.

The surface tension and structure of the $BMIMBF_4$-water and $BMIMPF_6$-water systems were studied at global mole fractions (number of ion pairs divided by the total number of molecules) ranging from 0.004 to 0.1 and from 0.001 to 0.03, respectively. Because of a propensity of the ions for the surface, the bulk concentration of the ionic liquid differs considerably from the global concentration. The bulk mole fractions were determined from the density profiles at the center of the slab (see Tables 1 and 2) and are a subject of statistical errors of roughly ten percent. The bulk concentration is higher in the case of $BMIMBF_4$ then in by $BMIMPF_6$, which is not surprising ($BMIMPF_6$ is more hydrophobic).

The surface tension in dependence on the global ionic liquid concentration is plotted in Fig. 7. We can see that the surface tension drops from that of the pure TIP4P/2005 water to lower values. In the case of $BMIMBF_4$ it reaches a shallow minimum and then rises again as the concentration increases. This anomalous behavior has been observed experimentally and we can semiquantitatively reproduce it by simulations. We have not detected any such increase for $BMIMPF_6$ in the range of studied concentrations. The interpretation, however, is not easy. The density profiles and other structure data look qualitatively the same irrespective on the concentration. The ionic liquid at low concentrations acts as a surfactant (because of hydrophobic butyls; anions then follow the cations because of electro-neutrality). In other words, energy is gained if the ions move to the surface. As the concentration increases again, the surface layer becomes saturated, and "normal" moderate increase of surface tension of electrolytes is re-established, a phenomenon traditionally explained by strong ion-water association. Here the bulk concentration of $BMIMPF_6$ is much lower at the same global concentration (shown in the graphs) and is not sufficient to cause the surface tension increase unlike more soluble $BMIMBF_4$.

4.2. MD with a polarizable force field

The structure and surface tension of the $BMIMBF_4$ aqueous solutions were studied at mole fractions ranging from 0.002 to 0.05. Figure 8 shows a typical snapshot from polarizable MD simulations at the lowest concentration of the ionic liquid. The side view demonstrates the slab geometry with two solution/vapor interfaces to which both cations and anions tend to segregate. A snapshot from a simulation of the most concentrated solution is presented in Fig. 9. It shows a top view of the surface which is covered with $[BMIM]^+$ and $[BF_4]^-$ ions.

Figure 10 depicts the density profiles for the two extreme concentrations investigated (0.002 and 0.05 mole fraction). At all concentrations both ions exhibit a much more pronounced surface propensity than in the case of nonpolarizable model. At 0.002 mole fraction the ions practically do not visit the bulk region of the slab on the timescale of the simulation. At 0.05 mole fraction ions populate the whole slab with peak surface enhancement of a factor of 3–4 compared to the bulk. It can be also seen from Fig. 10—similarly as in the nonpolarizable case—the peak of the terminal carbon of the aliphatic chain of the $[BMIM]^+$ cations is shifted toward the vapour phase by ~5 Å compared to the nitrogen peak. This indicates that these cations are strongly oriented in the surface layer with the hydrophobic chain pointing away from the bulk solution. In contrary, the positively charged ring points toward the solution and its density peak overlaps with that of the counter-anions.

Accounting for the (partial) charges on the individual atoms the above density profiles can be translated to charge profiles displayed in Fig. 11. At 0.002 mole fraction the interfacial charge distribution is dominated by oriented water molecules, with positive dangling hydrogens pointing into the gas phase. Nevertheless, the signal from the ions is non-negligible with the cationic and anionic signals perfectly cancelling each other (in the non-polarizable simulation, the cancelling is only partial at low concentrations). At 0.05 mole fraction the charge distribution in the solution is already dominated by the $[BMIM]^+$ and $[BF_4]^-$ ions. Again, the cationic and anionic distributions cancel each other.

Within simulations employing a polarizable force field the induced dipoles also contribute to the electrostatics of the systems. Fig. 12 depicts the induced dipoles on the cations, anions, and water molecules for the two extreme ionic liquid concentrations investigated. As in the case of charge distributions the induced dipoles at low concentration are dominated by water contribution, while at the higher concentration the contribution from the ions (particularly the more polarizable anions) becomes important. Generally speaking, the induced dipoles tend to cancel the effect of the permanent charges.[50] It is rather difficult to fully converge the distribution of induced dipoles, hence the slight deviation from antisymmetry with respect to the center of the slab in Fig. 12.

Finally, we have used the simulations with a polarizable force field to evaluate surface tension as a function of ionic liquid concentration in the 0.002–0.05 mole fraction range (Table 3 and Fig. 7). Despite the fact that the present water potential (POL3) underestimates surface tension the experimental trend upon adding the ionic liquid is well reproduced. Namely, surface tension steeply decreases up to about 0.02 mole fraction, after which it starts to slowly rise again.

5. Conclusions

We performed molecular dynamics simulations with both non-polarizable and polarizable force fields for aqueous solutions of $BMIMBF_4$ and $BMIMPF_6$ ionic liquids. We reproduced the experimentally observed decrease in surface tension in dilute solutions of ionic liquids and related it to the surface propensity of hydrophobic butylmethylimidazolium cations, accompanied by anions to re-establish local charge neutrality. The butyl chains tend to point towards vacuum and the imidazolium rings are preferentially parallel to the surface. The increase in surface tension at higher concentrations was detected for a less hydrophobic

$BMIMBF_4$. Both the structure phenomena (butyl chains at the surface, surface tension vs. concentration curve) are more pronounced if a polarizable force field is used.

Acknowledgments

We gratefully acknowledge a support from the Granting Agency of the Czech Republic (grant 203/07/1006) and the computing facilities from Czech Ministry of Education (Center for Biomolecules and Complex Molecular Systems, grant LC512). B. M. acknowledges support from the Granting Agency of the Czech Republic (grant 203/05/H001).

Appendix: Cutoff corrections in the slab geometry

We write the total interatomic potential as

$$u_{ij} = u_{ij,\mathrm{short}} + \Delta u_{ij} \tag{8}$$

In particular, MACSIMUS [39] implements

$$\Delta u(r) = \begin{cases} 0, & \text{for } r \in [0, c_1] \\ u(r) - C(r^2 - c_2^2)^2, & \text{for } r \in [c_1, c_2] \\ u(r), & \text{for } r \in [c_2, \infty] \end{cases} \tag{9}$$

where constants C and c_1 are determined from the cutoff c_2 and the potential so that both $\Delta u(r)$ and its derivative $\Delta u'(r)$ is continuous for all positive r.

Let $\zeta_i(z)$ denote the z-density profile of atom i. The correction in the averaged potential energy E (residual internal energy) can be approximated by integration over all (assuming uncorrelated) positions of pairs ij and then by summing over all pairs

$$\Delta E = \sum_{i<j} \frac{\int \zeta_i(z_i)\mathrm{d}\vec{r}_i \int \zeta_j(z_j)\mathrm{d}\vec{r}_j \, \Delta u_{ij}(r_{ij})}{\int \zeta_i(z_i)\mathrm{d}\vec{r}_i \int \zeta_j(z_j)\mathrm{d}\vec{r}_j} \tag{10}$$

This can be partly integrated and rearranged to a 3-dimensional integral,

$$\Delta E = \sum_{i<j} \frac{\int \zeta_i(z_i)\mathrm{d}z_i \int \zeta_j(z_j)\mathrm{d}z_j I_{ij}(|z_i - z_j|)}{L_x L_y \int \zeta_i(z_i)\mathrm{d}z_i \int \zeta_j(z_j)\mathrm{d}z_j} \tag{11}$$

where

$$I_{ij}(z) = \int_0^\infty 2\pi r \mathrm{d}r \Delta u_{ij}(\sqrt{r^2 + z^2}) = 2\pi \int_0^{1/\max(c_1, z)} \frac{\mathrm{d}t}{t^3} \Delta u_{ij}(1/t) \tag{12}$$

In practical evaluation we first calculate, for all atom type pairs *ij*, tables $I_{ij}(z)$ for z running in the same grid of 1 Å as $\zeta_i(z)$ (by a fourth-order Gaussian integration over dt), then the integrals over $\mathrm{d}z_i$ and $\mathrm{d}z_j$ are numerically evaluated by the trapezoidal rule with the same grid as $\zeta_i(z)$.

For determining the surface tension correction, term *u* in the above formulas should be replaced by

$$\Delta u \quad \longrightarrow \quad \frac{L_z}{4V} \frac{x^2 + y^2 - 2z^2}{r} \Delta u'(r) \tag{13}$$

and then

$$I_{ij}(z) = \frac{L_z}{4V} 2\pi \int_0^{1/\max(c_1, z)} \frac{\mathrm{d}t}{t^2} [1/t^2 - 3z^2] \Delta u'_{ij}(1/t) \tag{14}$$

in (11) gives $\Delta\gamma$ instead of ΔE.

Table 1: Surface tension of $BMIMBF_4$ as a function of ionic liquid mole fraction obtained from molecular dynamics simulations with a non-polarizable force field. The values in parentheses are estimated standard errors in the units of the last significant digits. Lennard-Jones cutoff corrections of about 3.5–4 mN/m are included.

Global mole fraction	Bulk mole fraction	γ / (mN/m)
0	0	59.0(8)
0.004	0.0035(5)	56.3(17)
0.01	0.0063(5)	56.4(10)
0.0015	0.010(2)	50.3(15)
0.02	0.0066(10)	53.1(10)
0.025	0.018(2)	53.5(9)
0.03	0.024(2)	55.0(10)
0.04	0.033(2)	56.4(19)
0.05	0.046(4)	54.2(10)

Table 2: Surface tension of $BMIMPF_6$ as a function of ionic liquid mole fraction obtained from molecular dynamics simulations with a non-polarizable force field.

Global mole fraction	Bulk mole fraction	γ / (mN/m)
0	0	59.0(8)
0.001	0.0007(2)	57.7(9)
0.002	0.0010(5)	61.0(8)
0.003	0.0013(5)	57.1(20)
0.004	0.0014(5)	58.1(8)
0.008	0.0044(20)	56.7(20)
0.01	0.031(10)	59.0(20)
0.02	0.0077(15)	55.1(9)
0.03	0.0106(10)	53.8(9)

Table 3: Surface tension of $BMIMBF_4$ as a function of ionic liquid mole fraction obtained from molecular dynamics simulations with a polarizable force field. The data do not contain the Lennard-Jones cutoff correction.

Bulk mole fraction	γ / (mN/m)
0.0022(6)	60.4(1)
0.0045(9)	54.8(2)
0.009(2)	53.9(1)
0.0219(25)	50.6(2)
0.0592(55)	52.8(2)

Figure captions:

Figure 1: Density profiles of $BMIMPF_6$; mole fraction of ionic liquid of 0.004 and 0.05 on the left and on the right site, respectively; green: nitrogens of $[BMIM]^+$; black: terminal carbon of the alkyl chain of $[BMIM]^+$; blue: phosphorus of $[PF_6]^-$; red: water oxygen.

Figure 2: Density profiles of $BMIMBF_4$; mole fraction of ionic liquid of 0.004 and 0.05 on the left and on the right site, respectively; green: nitrogens of $[BMIM]^+$; black: terminal carbon of the alkyl chain of $[BMIM]^+$; blue: boron of $[BF_4]^-$; red: water oxygen.

Figure 3: Charge density profiles of $BMIMBF_4$; black: cation, blue: anion, red: water, green: summary.

Figure 4: Charge density profiles of $BMIMPF_6$; black: cation, blue: anion, red: water, green: summary.

Figure 5: Orientational order of $BMIMBF_4$; mole fraction of ionic liquid of 0.004 and 0.05 on the left and on the right side, respectively; black: cosine of the angle between the cation and the surface normal, blue: the second Legendre polynomial of the angle between the imidazolium ring and the surface.

Figure 6: Orientational order of $BMIMPF_6$; mole fraction of ionic liquid of 0.004 and 0.05 on the left and on the right side, respectively; see caption of Fig. 5. for details.

Figure 7: Left: the simulated surface tension of $BMIMBF_4$ as a function of global concentration in the simulation box; full circles: non-polarizable model, open circles: polarizable model. Right: the simulated surface tension of $BMIMPF_6$ using non-polarizable model.

Figure 8: A typical snapshot from the polarizable MD simulation of the 0.002 mole fraction aqueous solution of $BMIMBF_4$ – side view with licorice representation of atoms.

Figure 9: A typical snapshot from the polarizable MD simulation of the 0.05 mole fraction aqueous solution of $BMIMBF_4$ – top view with van der Waals sphere representation of atoms.

Figure 10: Density profiles of boron of $[BF_4]^-$, terminal carbon of the alkyl chain and methylated nitrogen of $[BMIM]^+$, and water oxygen across the slab. The mole fraction of ionic liquid of 0.002 and 0.05 on the left and on the right site, respectively. The normalization is such that the integral under all curves is the same. Simulation with polarizable force field.

Figure 11: Charge profiles of $[BF_4]^-$, $[BMIM]^+$, and water across the slab. The mole fraction of ionic liquid of 0.002 and 0.05 on the left and on the right site, respectively. Simulation with polarizable force field.

Figure 12: Induced dipoles on the cations, anions, and water molecules across the slab for the global mole fraction of ionic liquid of 0.002 and 0.05 on the left and on the right site, respectively. Simulation with polarizable force field.

Figure 1:

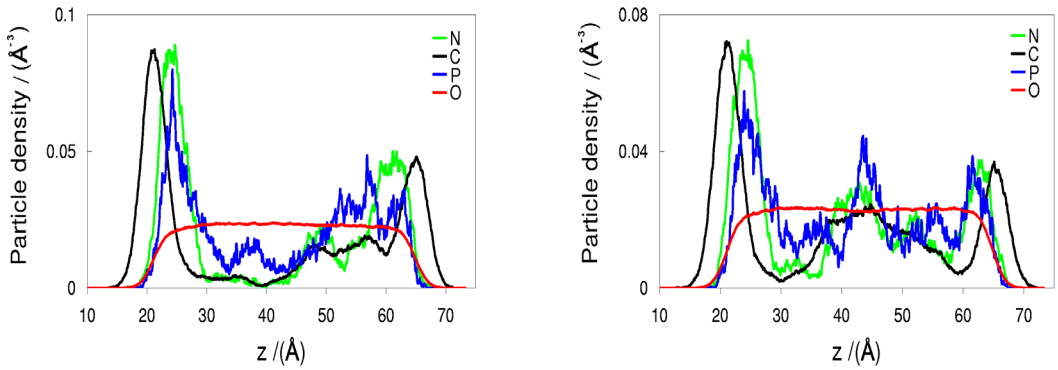
Particle density / (Å^{-3})
0.1
0.05
0
10
20
30
40
50
60
70
z /(Å)
N
C
P
O
Particle density / (Å^{-3})
0.08
0.04
0
10
20
30
40
50
60
70
z /(Å)
N
C
P
O

Figure 2:

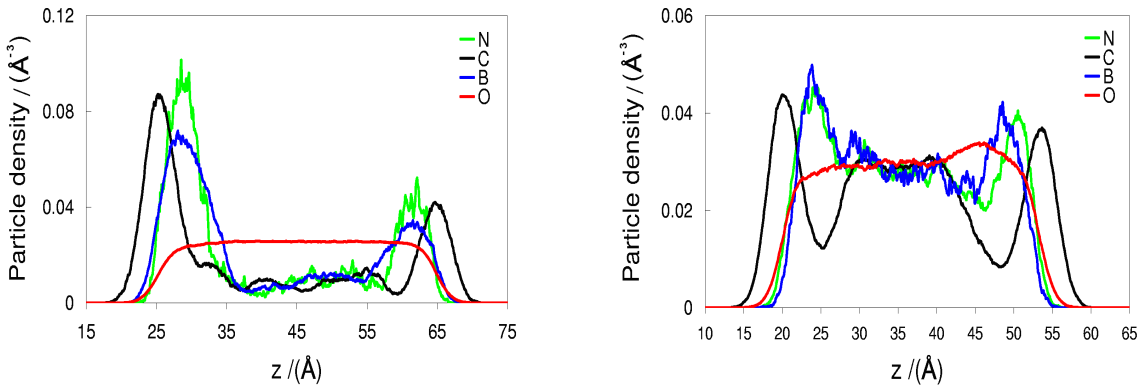
Particle density / (Å-3)
0.12
0.08
0.04
0
15
25
35
45
55
65
75
z /(Å)
N
C
B
O
Particle density / (Å-3)
0.06
0.04
0.02
0
10
15
20
25
30
35
40
45
50
55
60
65
z /(Å)
N
C
B
O

Figure 3:

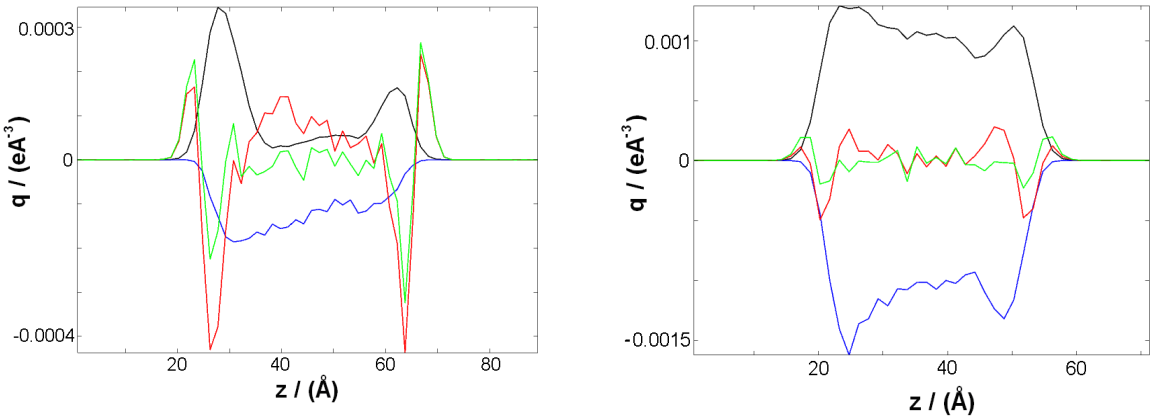

Figure 4:

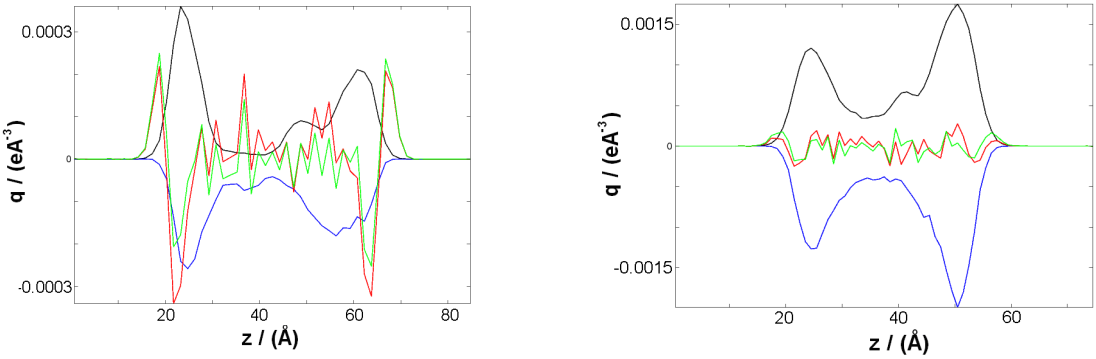

Figure 5:

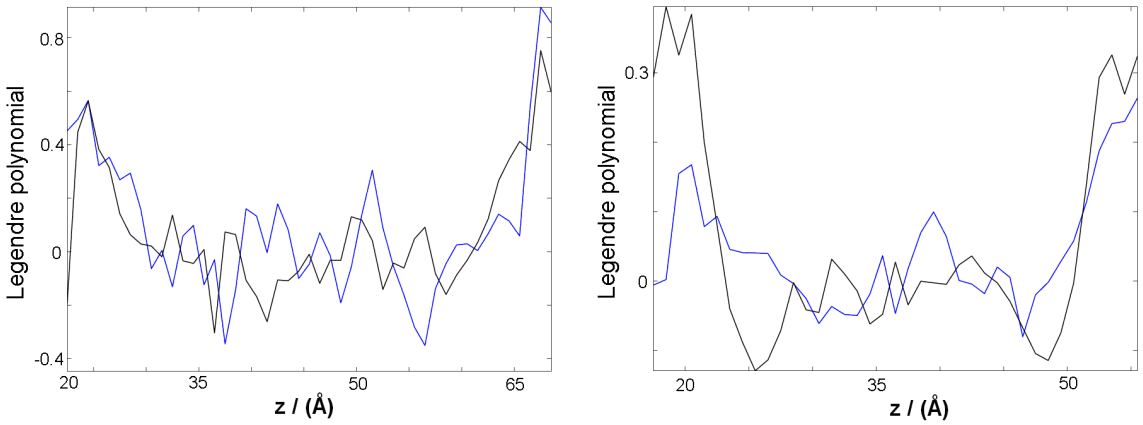
Legendre polynomial
0.8
0.4
0
-0.4
20
35
50
65
z / (Å)
Legendre polynomial
0.3
0
20
35
50
z / (Å)

Figure 6:

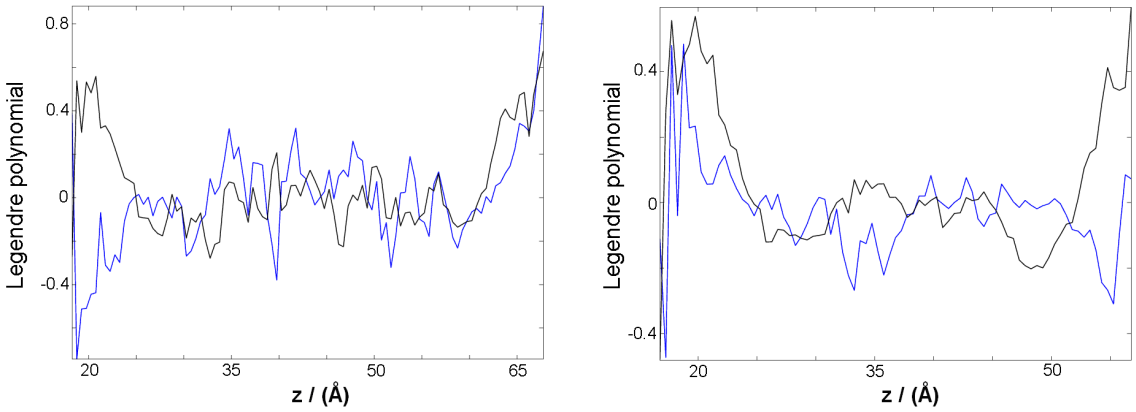
0.8
0.4
0
-0.4
Legendre polynomial
20
35
50
65
z / (Å)
0.4
0
-0.4
Legendre polynomial
20
35
50
z / (Å)

Figure 7:

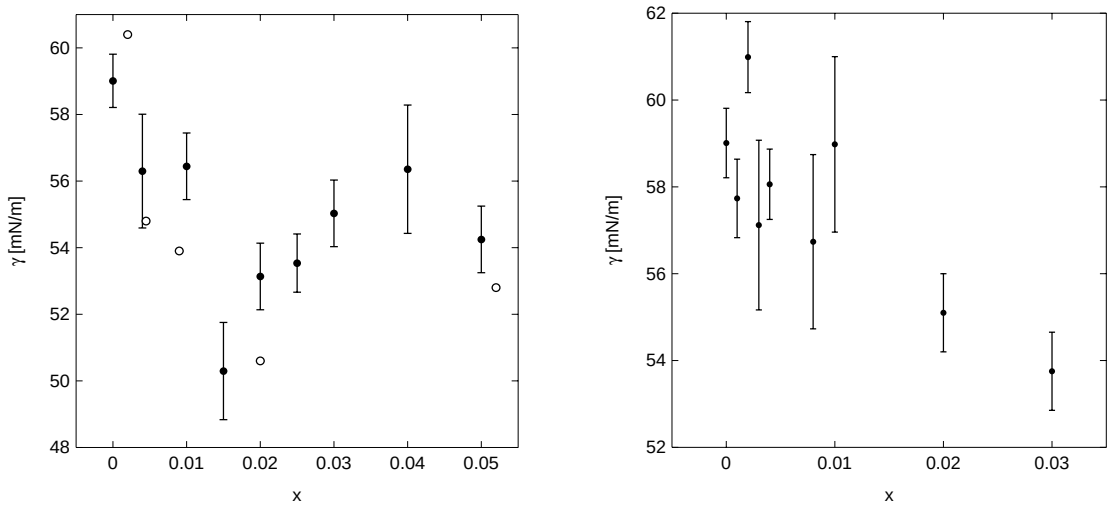
γ [mN/m]
x
60
58
56
54
52
50
48
0
0.01
0.02
0.03
0.04
0.05
62
60
58
56
54
52
0
0.01
0.02
0.03

Figure 8:

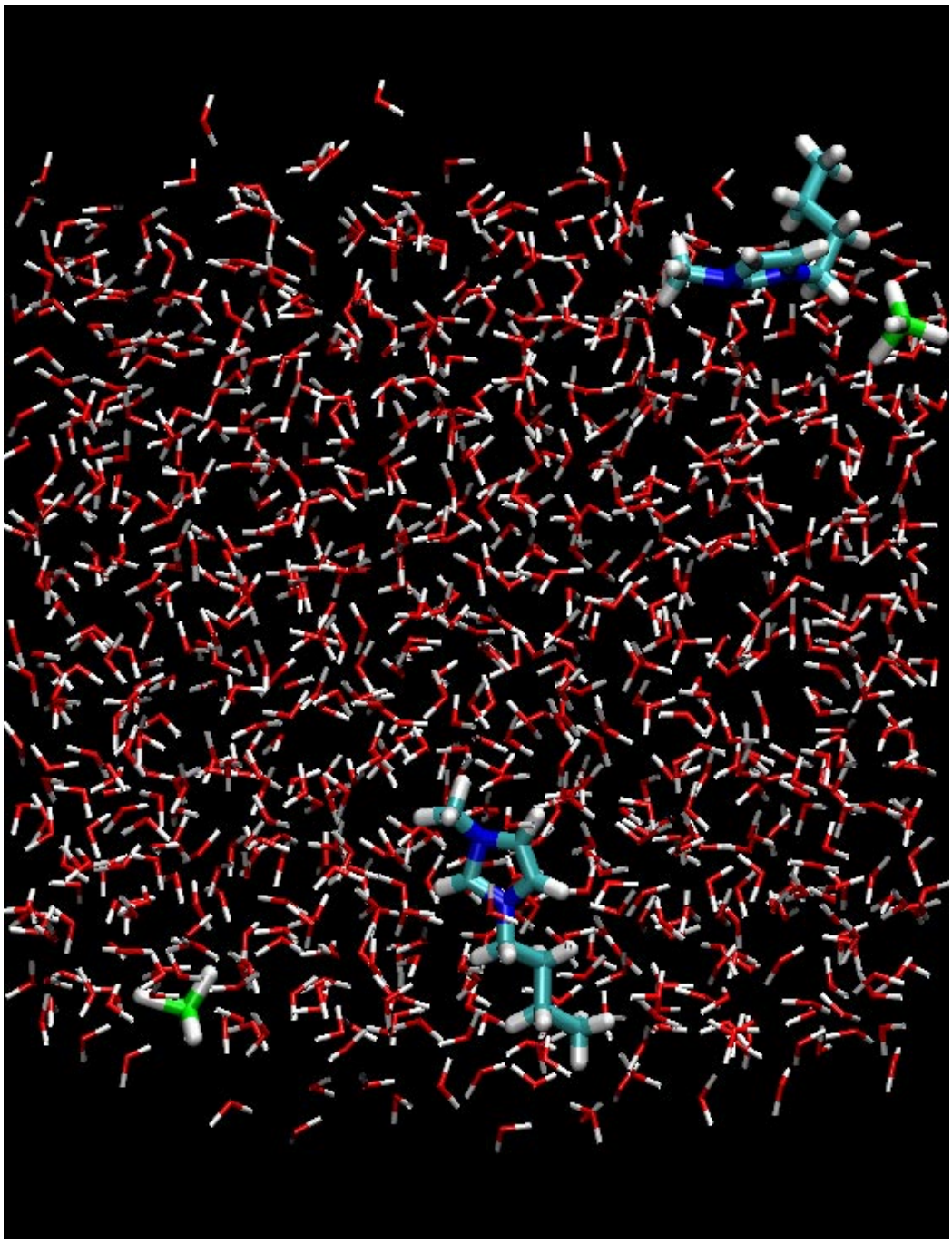

Figure 9:

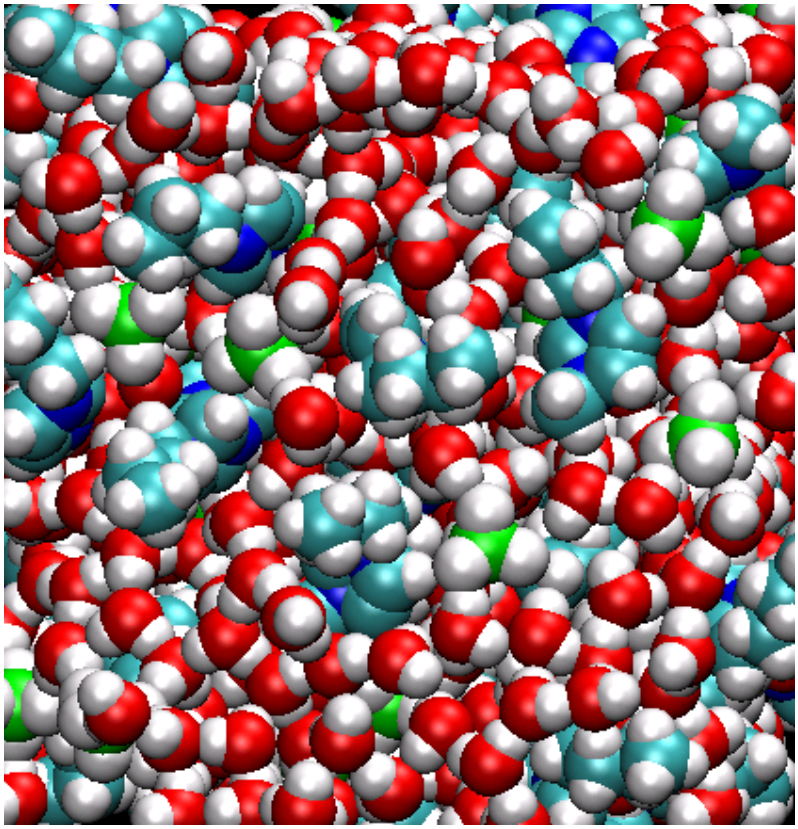

Figure 10:

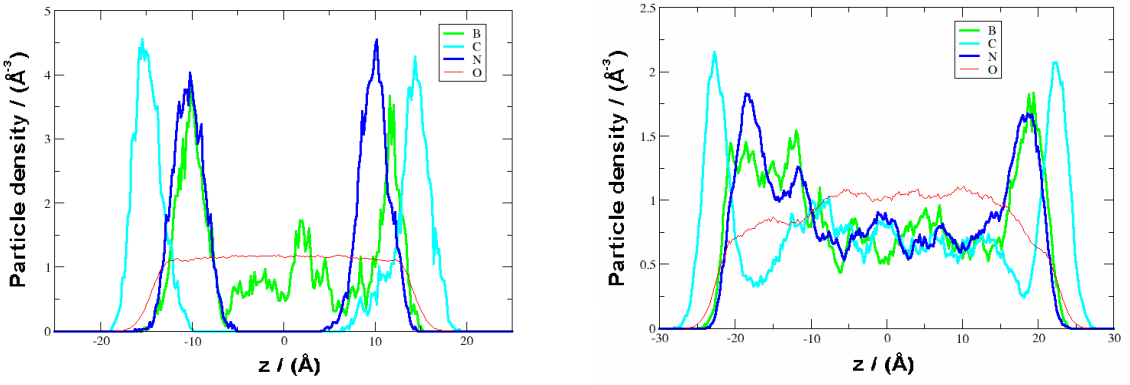

Figure 11:

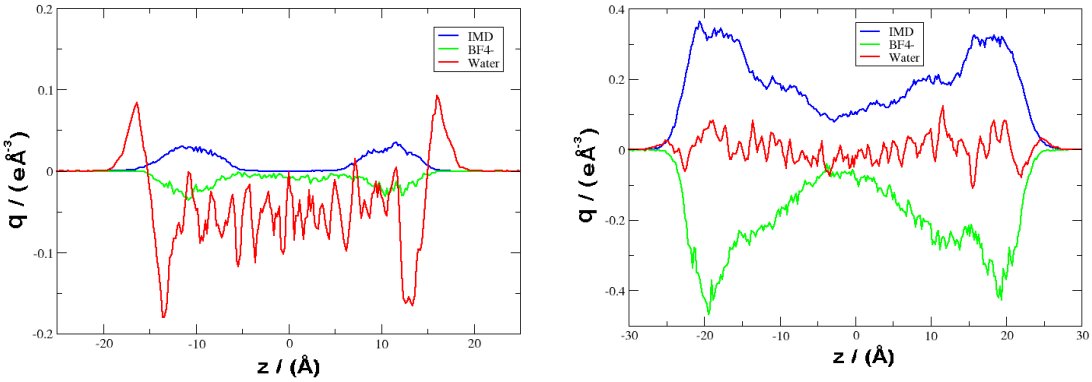

Figure 12:

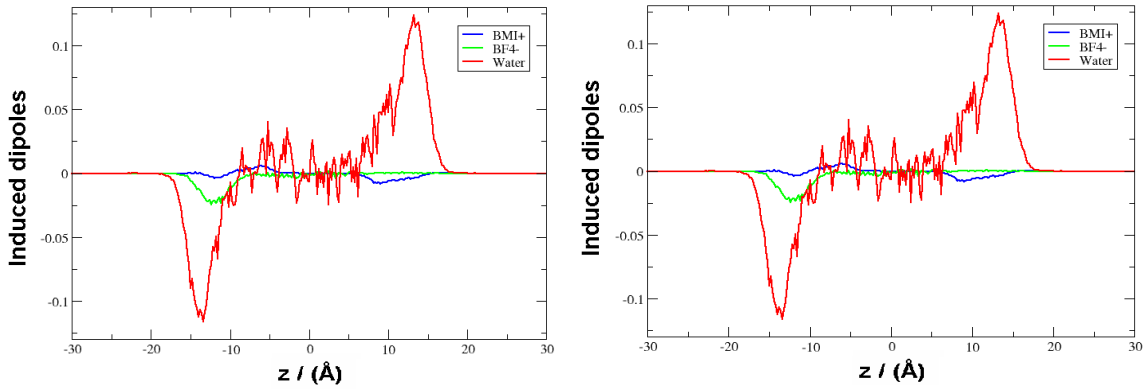
Induced dipoles
z / (Å)
BMI+
BF4-
Water
0.1
0.05
0
-0.05
-0.1
-30
-20
-10
0
10
20
30

References

[1] Endres, F.; Abedin, S. Z. E. *Phys. Chem. Chem. Phys.*, **2006**, 8, 2101.

[2] Welton, T.; *Chem. Rev*. **1999**, 99, 2071.

[3] G. Law, P.R.; Watson, A.J.; Carmichael, K.R.; Seddon, K. R. *Phys. Chem. Chem. Phys.* **2001**, 3, 2879.

[4] Solutskin, E.; Ocko, B.M.; Taman, L.; Kuzmenko, I.; Gog, T.; Deutsch, M. J. *Am. Chem. Soc.*, **2005**, 127, 7796.

[5] Bowers, J.; Butts, C.P.; Martin, P.J.; Vergara-Gutierrez, M.C.; Heenan, R.K. *Langmuir* **2004**, 20, 2191.

[6] Bowers, J.; Vergara-Gutierrez, M.C.; Webster, J.R.P. *Langmuir* **2004**, 20, 309.

[7] Sung, J.; Jeon, Y.; Kim, D.; Iwahashi, T.; Iomori, T.; Seki, K.; Ouchi, Y. *Chem. Phys. Lett.* **2005**, 406, 495.

[8]. Watson, P. W.; Law, G. *Chem. Phys. Lett.* 2001, 345, 1.

[9] Iimori, T.; Iwahashi, T.; Ishii, H.; Seki, K.; Hamaguchi, H.; Kim, D. *Chem. Phys. Lett.* **2004**, 389, 321.

[10] Baldelli, S. *J. Phys. Chem. B* **2003**, 107, 6148.

[11] Wang, Y.; Li, H.; Han, S. *J. Phys. Chem. B* **2006**,110, 24646.

[12] Hunt, P.A.; Gould, I.R. *J. Phys. Chem. A* **2006**, 110, 2269.

[13] Anthony, J.L.; Maginn E. J.; Brennecke, J.F. *J. Phys. Chem. B* **2001**, 105, 10949.

[14] Hanke, C.G.; Atamas, N.A.; Lynden-Bell, R.M. *Green Chem.* **2002**, 4, 107.

[15] Chaumont, A.; Schurhammer, R.; Wipff, G. *J. Phys. Chem. B* **2005**, 109, 18964.

[16] Chevrot, G.; Schurhamer, R.; Wipff, G. *Phys. Chem. Chem. Phys*. **2006**, 8, 4166.

[17] Lynden-Bell, R. M. Mol. Phys. **2003**, 101, 2625.

[18] Lynden-Bell, R. M.; Popolo, M. *Phys. Chem. Chem. Phys.* **2005**, 8, 949.

[19] Yan, T.; Liu, S.; Jiang. W.; Xueping, G.; Xiang, B.; Voth G.A. *J. Phys. Chem. B* **2006**,

110, 1800.

[20] Hanke, C.G.; Price, S.L.; Lynden-Bell, R.M. *Molecular Physics* **2001**, 99, 801.

[21] Andrade, J.; Böes, E.S.; Stassen, H. *J. Phys. Chem. B* **2002**, 106, 3546.

[22] Shah, J.K.; Brennecke, J.F.; Maginn, E.J. *Green Chemistry* **2002**, 4, 112.

[23] Shah, J.K.; Maginn, E.J. *Fluid Phase Equilibria* **2004**, 222, 195.

[24] Morrow, T.I.; Maginn, E.J. *J. Phys. Chem. B* **2002**, 106, 12807.

[25] Margulis, C.J.; Stern, H.A.; Berne, B.J. *J. Phys. Chem. B* **2002**,106, 12017.

[26] Lopes, J.N.C.; Deschamps, J.; Padua, A.H. *J. Phys. Chem. B* **2002**, 108, 2038.

[27] Urahata, S.M.; Ribeiro, M.C.C. *J. Chem. Phys.***2004**, 120, 1855.

[28] Liu, Z.; Huang, S.; Wang, W. *J. Phys. Chem. B* **2004**, 108, 12978.

[29] Lee, S.U.; Jung, J.; Young-Kyu, H. *Chemical Physics Letters* **2005**, 406, 332.

[30] Yan, T.; Burnham, C.J.; Del Popolo, M.G.; Voth, G.A. *J. Phys. Chem. B* **2004**, 108, 11877.

[31] Jungwirth, P.; Tobias, D. J. *Journal of Physical Chemistry B*, **2002**, 106, 6361.

[32] Jungwirth, P.; Tobias, D. J. *Chemical Reviews*, **2006**, 106, 1259.

[33] Chang, T.-M.; Dang, L.X. *Chem. Rev.* **2006**, 106, 1305.

[34] Welton, T.; Cammarata, L.; Kazarian, S.G.; Salter, P.A. Phys. Chem. Chem. Phys. **2001**, 2, 5192.

[35] Rivera-Rubero, S.; Baldelli, S. J. Am. Chem. Soc. **2004**, 126, 11788.

[36] Rivera-Rubero, S.; Baldelli, S.J. Phys. Chem. B **2006**, 110, 15499.

[37] Abascal, J.L.F.; Vega, C. *J. Chem. Phys.* **2005**, *123*, 234505.

[38] Benjamin, I. *J. Chem. Phys.* **1991**, *95*, 3698.

[39] L. Chen, J. Chem. Phys. **1995**, 103, 10214.

[40] Allen, M. P.; Tildesley, D. J. *Computer Simulation of Liquids*, Oxford University Press, Oxford, 1987.

[41] Yeh, I.-C.; Berkowitz, M. L. *J. Chem. Phys.* **1999**, *111*, 3155.

[42] Kolafa, J. http://www.vscht.cz/fch/software/macsimus/

[43] Zhang, Y.; Feller, S.E.; Brooks, B.R.; Pastor, R.W. *J. Chem. Phys.* **1995**, *103*, 10252.

[44] Essmann, U.; Perera, L.; Berkowitz, M.L.; Darden, T.; Lee, H.; Pedersen, L.G. *J. Chem. Phys.* **1995**, *103*, 8577.

[45] Ryckaert, J.P.; Ciccotti, G.; Berendsen, H.J.C. *J. Comp. Phys.* **1977**, *23*, 327.

[46] Wang, J.M.; Wolf, R.M.; Caldwell, J.W.; Kollman, P.A.; Case, D.A. *J. Comp. Chem.* **2004**, *25*, 1157.

[47] Caldwell, J. W.; Kollman, P. A. *J. Phys. Chem.* **1995**, *99*, 6208.

[48] Bayly, C.I.; Cieplak, P.; Cornell, W.D.; Kollman, P.A. *J. Phys. Chem.* **1993**, *97*, 10269.

[49] Case, D. A.; Darden, T. A.; Cheatham, T. E., III; Simmerling, C. L.; Wang, J.; Duke, R. E.; Luo, R.; Merz, K. M.; Wang, B.; Pearlman, D. A.; Crowley, M.; Brozell, S.; Tsui, V.; Gohlke, H.; Mongan, J.; Hornak, V.; Cui, G.; Beroza, P.; Schafmeister, C.; Caldwell, J. W.; Ross, W. S.; Kollman P. A. Amber 8; University of California: San Francisco, CA, 2004.

[50] Wick, C.D.; Dang, L.X.; Jungwirth, P. *J. Chem. Phys.* **2006**, *125*, 024706.